NeuroImage 213 (2020) 116692

Contents lists available at ScienceDirect

NeuroImage

journal homepage: www.elsevier.com/locate/neuroimage

The pontine-driven somatic gaze tract contributes to affective processing in humans

Jing Jun Wong [a,b,c,1], Dorita H.F. Chang [a,d,1], Di Qi [a,b,c], Weiwei Men [e], Jia-Hong Gao [f], Tatia M.C. Lee [a,b,c,g,h,*]

[a] State Key Laboratory of Brain and Cognitive Sciences, The University of Hong Kong, Hong Kong
[b] Laboratory of Neuropsychology, The University of Hong Kong, Hong Kong
[c] Laboratory of Social Cognitive and Affective Neuroscience, The University of Hong Kong, Hong Kong
[d] Department of Psychology, The University of Hong Kong, Hong Kong
[e] Center for MRI Research, Academy for Advanced Interdisciplinary Studies, Peking University, Beijing, 100871, China
[f] Center for MRI Research and McGovern Institute for Brain Research, Peking University, Beijing, 100871, China
[g] Institute of Clinical Neuropsychology, The University of Hong Kong, Hong Kong
[h] Center for Brain Science and Brain-Inspired Intelligence, Guangdong-Hong Kong-Macao Greater Bay Area, China

ARTICLE INFO

Keywords:
Pons
Emotion
Affective processing
fMRI
DTI
Functional connectivity

ABSTRACT

The relevance of subcortical structures for affective processing is not fully understood. Inspired by the gerbil retino-raphe pathway that has been shown to regulate affective behavior and previous human work showing that the pontine region is important for processing emotion, we asked whether well-established tracts in humans traveling between the eye and the brain stem contribute to functions beyond their conventionally understood roles. Here we report neuroimaging findings showing that optic chiasm-brain stem diffusivity predict responses reflecting perceived arousal and valence. Analyses of subsequent task-evoked connectivity further revealed that visual affective processing implicates the brain stem, particularly the pontine region at an early stage of the cascade, projecting to cortico-limbic regions in a feedforward manner. The optimal model implies that all intrinsic connections between the regions of interest are unidirectional and outwards from the pontine region. These findings suggest that affective processing implicates regions outside the cortico-limbic network. The involvement of a phylogenetically older locus in the pons that has consequences in oculomotor control may imply adaptive consequences of affect detection.

1. Introduction

Work toward understanding the mechanisms underlying affective processing have primarily focused on the roles of regions within the cortico-limbic circuitry, the default mode network (DMN), or the salience and emotion network (SEN). Despite the extensive work that has teased apart the roles of a large number of cortical regions for affective processing, data implicating the potential roles of subcortical regions of the brain for affective processing are scarce. In previous work, we found that the functional connectivity between the pons and several cortico-limbic affective structures was correlated with various self-reported affective measures (Lee et al., 2015). Clinical evidence from patients who exhibit uncontrollable (pathological) episodes of laughing and/or crying has implicated lesions of the basis pontis (Arif et al., 2005; Lee et al., 2003; Parvizi et al., 2009). Moreover, studies have identified that significant depressive symptoms can be observed over a third of patients suffering Parkinson's disease (Aarsland et al., 2009; Starkstein and Leentjens, 2008; Weintraub et al., 2003), a neurodegenerative disorder marked by a degeneration of the pons (Halliday et al., 1990; Jubault et al., 2009; Saeed et al., 2017; Seidel et al., 2015). Disruption to these regions hinders the production of serotonin which is well documented for its role in affective regulation (Berger et al., 2009; Canli and Lesch, 2007; Yohn et al., 2017).

The involvement of the pons and other brain stem structures for affective processing are further supported by findings in rodents, which have been frequently used as models for studying the neural substrates of human behaviors (Ellenbroek and Youn, 2016). Rodents not only share several prominent landmarks with humans (Snyder et al., 2018), the

* Corresponding author. Rm 656, The Jockey Club Tower, The University of Hong Kong, Pokfulam Road, Hong Kong.
E-mail address: tmclee@hku.hk (T.M.C. Lee).
[1] Both authors contributed equally to this work.

https://doi.org/10.1016/j.neuroimage.2020.116692
Received 23 November 2019; Received in revised form 25 February 2020; Accepted 26 February 2020
Available online 2 March 2020
1053-8119/© 2020 The Authors. Published by Elsevier Inc. This is an open access article under the CC BY-NC-ND license (http://creativecommons.org/licenses/by-nc-nd/4.0/).

neural correlates of affective behavior are also reflected in similar brain structures (Atsak et al., 2011; Jeon et al., 2010; Terburg et al., 2018). A study on Mongolian gerbils identified a specific subtype of intrinsically photosensitive retinal ganglion cells (RGCs) that were responsible for the delivery of serotonin-modulating signals to the dorsal raphe nucleus (DRN), which in turn influence serotonergic tone and affective behavior (Ren et al., 2013). Activity of the DRN-projecting RGCs is directly correlated with the behavioral state, and increased activity could remedy depressive-like behaviors triggered by light deprivation (Lau et al., 2011; Luan et al., 2011; Zhang et al., 2016). Similar findings were also observed in rats (Li et al., 2015), suggesting that understanding this DRN afferent pathway and how it contributes to serotonin release may reveal the mechanisms underlying the effects of light therapy for reducing symptoms of depression and seasonal affective disorder. The retino-raphe projections have also been shown to be involved in the processing of rapidly approaching and visually threatening stimuli in mice (Huang et al., 2017). Given that the relevant structures of interest for the current study (i.e. optic chiasm and the pons) are found in rodents, these findings further emphasize the need to explore the roles of subcortical structures in human affective processing, especially the processing of sadness and fear which are primitive emotions strongly indicated in the survival of an animal.

In humans, the raphe nucleus spans along the whole brain stem with the DRN located in the midbrain portion of the brain stem. Studies on humans have identified that the brain stem elicited significant activity during blue light stimulation (Vandewalle et al., 2009, 2007), concurrent to the peak photosensitivity of intrinsically photosensitive RGCs (Li et al., 2015). Considering these findings, a functionally analogous pathway between the optic chiasm and the brain stem may also exist in humans. Moreover, despite the apparent relevance of the pons for affective processing in humans, it is unknown as to whether it is implicated through feedback from cortico-limbic affective structures or at an earlier, pre-cortical stage.

In this study, we focus on the scarcely studied subcortical structures in the brain stem (i.e., the pons) and how they subserve affective processing. Taking into account the findings in rodents where the retino-raphe projection is involved in processing both sadness and fear, we chose to use stimuli of both positive (i.e. happy) and negative (i.e. sad and fear) valence in order to test whether affective valence is reflected differently in brain stem and cortical regions. We used stimuli from the Nencki Affective Picture System that have been shown previously to well elicit distinguishable discrete emotions (Riegel et al., 2016). Here, our aims were threefold. First, we used diffusion tensor imaging (DTI) to ask whether well-established tracts in humans, particularly those between the eye and the brain stem (inclusive of the pontine region and DRN), may serve functions beyond their conventionally understood roles, specifically in relation to affective processing. We asked whether individual measures of the tracts' diffusivity between the optic chiasm and the brain stem can predict affective measures of perceived arousal and valence. We hypothesized that the degree of anisotropy in the diffusion (fractional anisotropy; FA) along the fiber bundles identified between the optic chiasm and the brain stem would only be correlated with negative affective measures (i.e., sad and fear stimuli), in line with the findings in rodents. Secondly, we sought to examine the effective connectivity between the pons and cortico-limbic regions in order to understand how the pons functions in relation to upstream visual affective processing. In order to do so, we applied dynamic causal modelling (DCM) to task-based fMRI data. We posited that pons engagement would occur earlier than cortico-limbic affective structures based on the evidence that brain stem structures present significant activations when participants were stimulated with blue light (Vandewalle et al., 2009, 2007), suggesting a direct projection from the eyes. Third, we asked whether the cortico-limbic-pontine network is involved in general visual affective processing or only involved in processing specific emotions. We postulated that this network would be unique to the processing of stimuli of negative valence based on the improvement in depressive symptoms observed in rodents (Lau et al., 2011; Luan et al., 2011; Zhang et al., 2016).

2. Materials and methods

2.1. Experimental design

2.1.1. Participants

We recruited 70 healthy and right-handed participants (males = 35) without a history of psychiatric or psychological disorders via posters administered through Beijing Normal University and Peking University. This sample size has been shown to be sufficient for producing large effect sizes in the pons (Lee et al., 2015). We obtained written informed consent from all participants before the experiment. The study protocol was approved by the Human Research Ethics Committee for nonclinical faculties of The University of Hong Kong (EA1705023). All experimental procedures followed the Declaration of Helsinki. The final sample consisted of 64 participants (males = 30), aged between 19 and 28, who we included after excluding for baseline measures of general intelligence (Test of Nonverbal Intelligence, Fourth Edition, TONI-4), anxiety [Hospital Anxiety and Depression Scale (HADS)-Anxiety score], and depression [Hospital Anxiety and Depression Scale (HADS)-Depression score]. We excluded participants who scored a TONI general score that was one standard deviation beyond the average (one participant) or a HADS score greater than or equal to 11 on either the anxiety or depression subscale (five participants). We excluded two additional participants for all DWI-related analyses due to poor data quality as their data failed to undergo the preprocessing procedures implemented.

2.1.2. Procedure

The total procedure lasted approximately 3 h. We required participants to fill in their demographic information and complete a series of baseline behavioral measures (detailed in the Supplementary Materials) including anxiety and depression, general intelligence, and state and trait affect in randomized order before entering the scanner. MRI scans included anatomical T1-weighted images, task-based functional MRI (fMRI), and diffusion weighted imaging (DWI). Upon completion of the MRI scans, we asked participants to complete a post-scan image-rating task to acquire behavioral data on the perceived arousal and valence of each stimulus before dismissal (see Table 1 for a summary of all behavioral data).

Table 1
Descriptive statistics of all measures used in this study.

Variables	Mean	SD
Age (year)	23.84	2.27
General intelligence (TONI-4) (n = 63)	102.40	9.40
HADS-Anxiety	4.48	2.65
HADS-Depression	3.67	2.65
CAS-Positive affect	33.45	5.40
CAS-Negative affect	19.56	5.02
Arousal ratings		
Happy stimuli	3.84	1.48
Sad stimuli	3.81	1.48
Fear stimuli	4.01	1.59
Neutral stimuli	2.42	1.12
Valence ratings		
Happy stimuli	5.70	0.94
Sad stimuli	2.72	0.91
Fear stimuli	3.13	0.88
Neutral stimuli	4.29	0.79
Happy ratings for happy stimuli	4.19	1.25
Sad ratings for sad stimuli	3.76	1.26
Fear ratings for fear stimuli	3.73	1.32

All measures were calculated for the 64 participants included in this study, with the exception of IQ (TONI-4), which only has $n = 63$, as one participant reached the minimum requirement for inclusion but had an incomplete score.

2.2. fMRI stimuli and task

The fMRI task required participants to passively view blocks of images of varying affect. The stimuli were selected from the Nencki Affective Picture System (Marchewka et al., 2014) (NAPS) containing 1356 images. All of the images were sorted into four affect groups (i.e., fear, happy, neutral, and sad) based on findings from Riegel and colleagues (Riegel et al., 2016). A subset of 510 images were initially rated by participants in a small pilot study using six independent 7-point Likert scales on affect (i.e., anger, fear, disgust, happiness, sadness, and surprise) and the Self-Assessment Manikin 9-point scale on two affective dimensions [i.e., arousal and valence (Bradley and Lang, 1994)]. The final set of stimulus items comprised 192 images, consisting of 48 images for each affect (i.e., fear, happy, neutral, and sad). The 48 images belonging to each affect group were rated highest on their corresponding affect (i.e. happy) while having low ratings for the other irrelevant affect categories (i.e. anger, fear, disgust, sadness, and surprise). Each image had a matched "masked" variation (i.e., "masked stimuli") generated by arbitrarily scrambling the x- and y-position of individual pixels. All images (both original and masked stimuli) were then normalized in terms of their overall luminance.

Within the scanner, we presented images in a block design using E-Prime (Psychology Software Tools, Sharpsburg, PA; RRID:SCR_009567). Participants completed a total of 6 runs, with each run consisting of eight blocks of images separated by a fixation cross (white cross on a black background) lasting 10 s. The eight blocks of images comprised four blocks corresponding to each of the main affect conditions (i.e. happy, sad, neutral, fear), and four blocks corresponding to the masked stimuli conditions (i.e. happy-mask, sad-mask, neutral-mask, fear-mask). Block order was presented in an interleaved manner, such that a main affect condition will always be followed by a masked stimuli condition. The masked stimuli condition is not yoked with the main affect condition. Each block consisted of eight randomized images presented for 3.5 s, followed by black screens lasting 0.25 s, lasting a total of 30 s. Participants were given 10 s of fixation cross between blocks, as well as a brief reset between runs, in order to allow them to return to a baseline affective state. Participants were instructed to attend to the images presented but no responses were required. We monitored each participants' wakefulness and attention via a live video camera typically used for eye-tracking (although no eye-tracking data was acquired for this particular experiment). Between each run, we communicated with the participant and provided short breaks upon request.

2.3. Post-scan image-rating task

Participants were requested to complete this task after they have completed the MRI scanning procedure. We generated the image-rating task using custom software written in MATLAB R2015b (Mathworks; RRID:SCR_001622) and extensions from the Psychtoolbox Version 3.0.14 [(Brainard, 1997; Pelli, 1997); RRID:SCR_002881]. This task was designed to verify that the fMRI task stimuli were eliciting the intended affects. It was further important to perform this task only after the completion of the MRI scan to ensure that the fMRI data were free of unintended stimulus adaptation effects or other subject demand characteristics. The participants were presented a total of 192 stimuli on the computer screen separated by five question screens which require participant response. These 192 images corresponded to the original stimuli presented in the fMRI task, but were presented in a random order. Each trial consisted of a picture presentation (3.5 s), followed immediately by five questions, each presented individually [adapted from Riegel and colleagues (Riegel et al., 2016)]. With no right or wrong answers, we asked participants to rate each stimulus based on their emotional feelings as they viewed each image. The rating task for each stimulus involved five measures: (1) happiness on a 7-point scale, (2) sadness on a 7-point scale, (3) fear on a 7-point scale, (4) arousal Self-Assessment Manikin on a 9-point scale, and (5) valence Self-Assessment Manikin on a 9-point scale. We explained to the participants that the 7-point emotional scale of happiness, sadness, and fear ranges from 1 (representing total absence of the given emotion) to 7 (representing the highest intensity of the emotion). For the Self-Assessment Manikins, participants were instructed that the arousal scale ranged from calm to excited, while the valence scale ranged from unpleasant to pleasant.

2.4. MRI acquisition parameters

MRI data for all participants were obtained at Peking University using a 3.0 T Siemens Prisma scanner equipped with a 64-channel head coil. High-resolution anatomical T1-weighted images were acquired using a magnetization-prepared rapid gradient echo (MP-RAGE) sequence [192 contiguous slices, echo time (TE) = 2.98 ms, repetition time (TR) = 2530 ms, inversion time (TI) = 1100 ms, matrix = 448 × 512, FOV = 224 × 256 mm, flip angle = 7°, voxel size = 0.5 × 0.5 × 1 mm] with generalized autocalibrating partial parallel acquisition (GRAPPA) and an in-plane acceleration factor of 2. We instructed participants to keep their eyes closed without falling asleep during this scan.

To avoid potential fatigue effects, DWI data collection was shortened by collecting from slices capturing the optic chiasm and the whole of the pons (Fig. 1A) rather than the whole brain. A readout-segmented echo-planar imaging (EPI) sequence (30 contiguous slices, TE = 64 ms, TR = 3900 ms, matrix = 98 × 98, FOV = 196 × 196 mm, flip angle = 180°, voxel size = 2 × 2 × 2 mm) with GRAPPA and an in-plane acceleration factor of 2 was used to acquire the DWI data. The DWI data consisted of 4 non-diffusion weighted references (b = 0 s/mm^2) and 30 diffusion-encoding gradient directions (b = 1000 s/mm^2). Participants were also instructed to keep their eyes closed without falling asleep during this scan.

We collected task-based fMRI data using a multiband EPI sequence (90 contiguous slices, 166 vol, TE = 30 ms, TR = 2000 ms, matrix = 124 × 124, FOV = 198 × 198 mm, flip angle = 90°, voxel size = 1.6 × 1.6 × 1.6 mm). This sequence used the controlled aliasing in parallel imaging results in higher acceleration (CAIPIRINHA) technique with an in-plane acceleration factor of 2 and a multiband factor of 3. Each participant completed a total of six runs of task-based fMRI. During this procedure, participants were instructed to complete the image viewing task as detailed in the fMRI Stimuli and Task section.

2.5. Quantification and statistical analysis of DWI data

2.5.1. Fiber tractography

DWI data preprocessing was performed using mrDiffusion tools implemented in the Stanford VISTA Lab's open-source VISTASOFT package (Stanford University, Stanford, CA, USA, http://vistalab.stanford.edu/software/). We removed eddy-current distortions and participant motion with an algorithm using a 14-parameter nonlinear co-registration based on an expected model of eddy-current distortions from the phase-encoding direction during data acquisition (Rohde et al., 2004). We excluded two additional participants for all DWI-related analyses due to poor data quality as their DWI data could be re-aligned and segmented during the preprocessing procedures implemented within the VISTASOFT package.

In this study, we elected to use both deterministic and probabilistic tractography methods as they have been demonstrated to exhibit different accuracy and sensitivity in fiber identification and diffusivity measures depending on the region of interest (Hu et al., 2011; Sarwar et al., 2019; Schlaier et al., 2017). Deterministic tractography was computed using a streamline tracking algorithm (Basser et al., 2000; Mori et al., 1999) (STT) with a fourth-order Runge-kutta path-integration method (Press et al., 1988) (Step Size = 1 mm, Angle Threshold = 45°, FA Threshold = 0.1, Length Threshold = 20 mm). Probabilistic fiber identification was performed using default sampling parameters in ConTrack (Sherbondy et al., 2008) with the following exclusion criteria: (i) bending angles beyond 130° for a single step (step size = 1 mm); (ii)

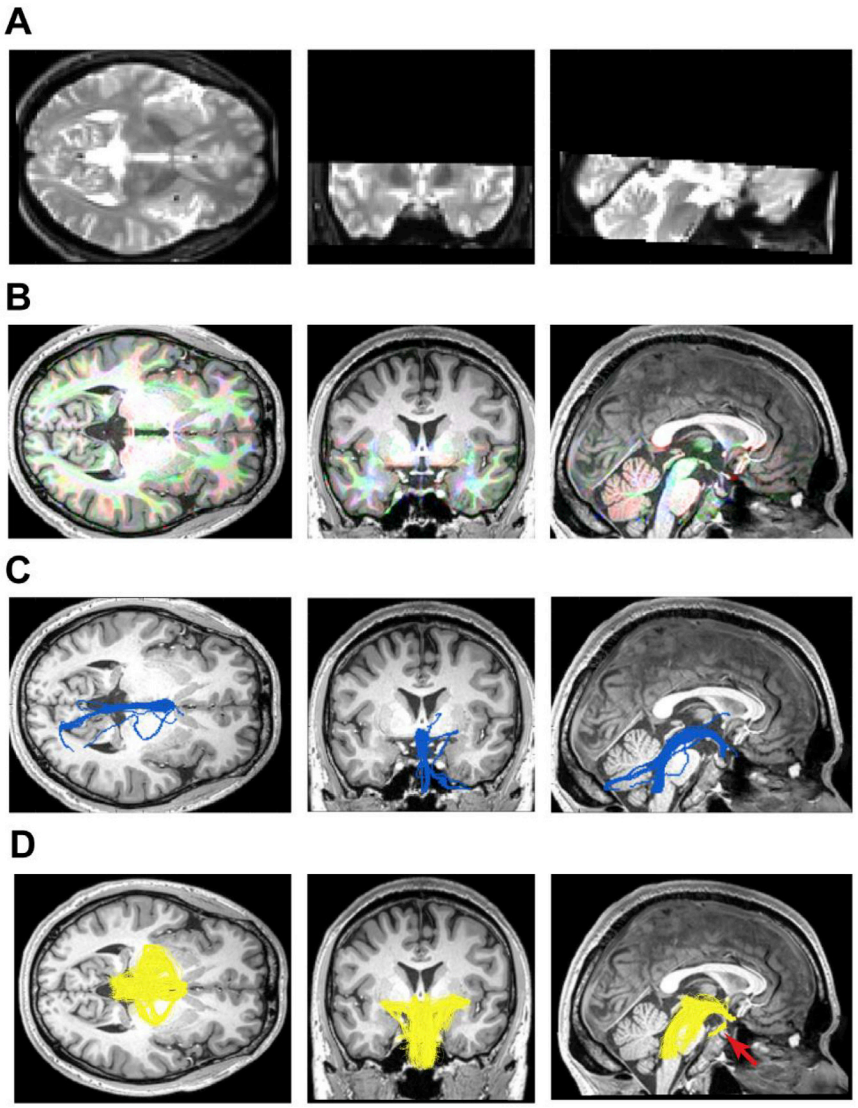

Fig. 1. DWI data and fiber tractography output. (**A**) The field of view (FOV) of the DWI data collected for a single subject. (**B**) RGB vector map overlaid on the T1 image of a single subject. (**C**) Deterministic fiber-tracking output of a single subject. (**D**) Probabilistic fiber-tracking output of a single subject. An additional fiber bundle that extends into pontine region that is not identified from deterministic tractography is indicated with a red arrow.

pathways that stepped through grey matter regions or exceeded 300 mm; and (iii) pathways without an end point in both ROIs. The algorithm sampled 100,000 pathways between the two ROIs, and we selected 10, 000 of the top scoring pathways from each analysis as the representation of the fiber bundle.

For both methods, we used a 4-mm radius sphere centered at the optic chiasm [MNI: (0.2 4.7–21.4) (Baroncini et al., 2012)] as a seed ROI to initiate the tractography process. This positioning of this seed was verified by manual inspection of each subject's T1-weighted image, following back-transformation of the data from MNI to native space prior to entering the data into tractography analyses (in native space). We selected this ROI because the identified retino-raphe tract in gerbils passed through the optic chiasm and because it is not possible to track directly behind the eyes due to inherent signal loss in that area. We set the end point as a mask spanning the full brain stem to ensure a comprehensive coverage of the subcortical structures of interest including the whole pontine region and the DRN based on findings in both humans (Arif et al., 2005; Lee et al., 2015, 2003; Parvizi et al., 2009) and gerbils (Li et al., 2015; Ren et al., 2013). We extracted this mask from the Harvard-Oxford probabilistic subcortical atlas (Desikan et al., 2006; Frazier et al., 2005; Goldstein et al., 2007; Makris et al., 2006; Mazziotta et al., 2001) and manually inspected it by overlaying on each subject's T1-weighted image. In order to ensure that we did not capture unintended influences from the superior colliculi (due to their known roles in saccadic orienting), we defined for each subject, their superior colliculi by means of manual inspection, and subtracted voxels defining this region from those defining brain stem ROI. Tracked fibers must pass through the optic chiasm ROI and the brain stem ROI. As a control comparison, we performed additional tracking of the optic tract between the optic chiasm and the thalamus. The optic tract serves as an interesting comparison as we expect a tract serving the traditional retinogeniculo system to be unrelated to affective processing. The thalamus ROI was also extracted from the Harvard-Oxford probabilistic subcortical atlas and manually verified for each subject through their T1-weighted image.

2.5.2. *Measures of diffusivity*

We elected to use FA, an index depicting the anisotropic diffusive movement of water molecules, to evaluate the tissue properties of the identified tracts. FA is widely used as a measure of white matter coherence (e.g. axon diameter, fiber density, and myelination), and has been shown to correlate with behavior and cognitive abilities in both healthy and depressed participants (Deutsch et al., 2005; Hoptman et al., 2004;

Nobuhara et al., 2006; Silveri et al., 2006). Briefly, a single FA value for each fiber group identified correspond to the average of values extracted at 30 equally spaced notes between the starting and ending ROIs. A Gaussian kernel is used to estimate the FA at each extraction point, with fibers nearer the center contributing more than the surrounding ones. In this manner, we extracted FA values for each participant for both the optic chiasm to brain stem tract and the optic chiasm to thalamus tract. FA values acquired from these tracts were then correlated (using a Spearman-Rho correlation) to their corresponding behavioral measures (i.e., intelligence, anxiety and depression, and state and trait affect) and results collected from the image-rating task to ascertain the role of the identified fiber groups.

2.6. Quantification and statistical analysis of fMRI data

2.6.1. Functional architecture

We included all 64 participants in the fMRI data analyses. We initially analyzed task-based fMRI data to identify regions of significant activation when viewing affect-related images compared to masked images. We then included significant activations signifying regions responsible for processing visual affective stimuli for the model generation for effective connectivity analysis. We used DCM to determine the directionality of the intrinsic connections between the pontine region and ROIs, as well as the modulatory effects of different affective stimuli (i.e., fear, happy, neutral, and sad).

2.6.2. Task-based fMRI data analysis

We preprocessed and analyzed task-based fMRI data using Statistical Parametric Mapping (SPM12; Wellcome Centre for Human Neuroimaging, Institute of Neurology, UCL, http://www.fil.ion.ucl.ac.uk/spm; RRID:SCR_007037). We applied SPM algorithms for slice-timing correction, realignment to T1-weighted anatomical reference, and unwarping based on estimated field map data to EPI images of individual participants. Following these steps, we applied the anatomical co-registration to the EPI images, and we used the parameters generated from the SPM segmentation procedure for normalization to the MNI space. We utilized an isotropic 3-mm full-width Gaussian kernel at half-maximum for smoothing. Statistical analysis was based on a generalized linear model (GLM). We assigned a square-wave regressor to each condition to be convolved with the hemodynamic response function and motion parameters. Also, we removed low-frequency components using a high-pass filter with a cutoff frequency of 1/128 Hz, and accounted for serial autocorrelations using a first-order autoregressive model with a coefficient of 0.2. A second-level analysis conducted using ANOVA identified regions of activation when viewing affect-related images (unmasked stimuli versus masked stimuli). From this contrast, we identified ROIs as significant clusters of activation ($p_{(FDR)} = 0.05$) and assigned a corresponding anatomical label using the automated anatomical labeling implemented in SPM (Tzourio-Mazoyer et al., 2002) and xjView (http://www.alivelearn.net/xjview; RRID:SCR_008642). Raw beta values were extracted using MarsBaR region of interest toolbox for SPM (http://marsbar.sourceforge.net/; RRID:SCR_009605), by computing the means of all voxels within each of the seven ROIs (5-mm radius spheres as defined for the DCM procedures) for each of the affect conditions (i.e. happy, sad, neutral, and fear). These extracted beta values were used to perform a Spearman-Rho correlation with the behavioral measures.

2.6.3. Effective connectivity analysis

We evaluated effective connectivity among our ROIs using DCM implemented in SPM12 (Friston et al., 2003; Stephan et al., 2010). In order to generate a meaningful model, we decided not to include in our model, all significant clusters retrieved from the GLM results above, but rather included only the most robust clusters selected after applying a stringent thresholding criterion ($p_{(FWE)} = 0.05$, cluster threshold = 10 voxels; Table 2A). In addition to GLM-thresholded ROIs, we included a set of a-priori selected ROIs that have been deemed to be particularly relevant to affective processing based on previous work (Lee et al., 2015; Sabatinelli et al., 2011). This included the pons for our a-priori hypothesis (Lee et al., 2015); the OFC and mPFC due to their intricate involvement with the amygdala within the SEN and their relevance to visual-affective processing (Adolphs, 2002; Cardinal et al., 2002; Phillips et al., 2003; Rolls, 2004); the amygdala because it is an important structure in affective processing and in particular the relevance to fear, one of the affective categories in this study (Adolphs, 2008, 2002; Davis and Whalen, 2001). The coordinates of these ROIs are summarized in Table 2B. Note that all of these additional ROIs were also identified in the second-level analysis above at the initial threshold ($p_{(FDR)} = 0.05$).

We used a 5-mm radius sphere to extract the first eigenvariate of all activated voxels (for the contrast between unmasked and masked stimuli; $p < 0.05$, uncorrected). The GLM-thresholded ROIs were centered on the local maxima (Table 2A). The a-priori selected ROIs were centered on coordinates reported by previous work [Table 2B (Lee et al., 2015; Sabatinelli et al., 2011)]. Bilateral ROIs contained two spheres centered at the corresponding coordinates with all contents extracted together.

A total of 75 models were constructed and compared (while treating each model as an individual family) using random effects Bayesian model selection (Friston et al., 2007), which favors models with both optimal complexity and fitting. The 75 models varied in intrinsic connections, had affective modulatory effects on these intrinsic connections, and also had affective modulatory effects directly on each of the ROIs. Based on our a-priori that the pons should be involved earlier than cortical structures due to a relatively direct pathway for transferring information, we constructed models primarily by considering the pons as the primary central node and varying the intrinsic connections with the other ROIs (testing both unidirectional and bidirectional connections), as well as the interconnections between these ROIs. We considered all types of affective modulation (i.e., happy, sad, neutral, and fear) without varying them among these 75 models (i.e., all affects were applied to each of the modulation of intrinsic pathways).

Once we acquired the optimal model (i.e. Model 26) from the Bayesian model selection process, we further explored whether the type of affect modulation would yield a more accurate model. Model 26 was adapted by keeping the intrinsic connections consistent while varying the four types of affective modulation (i.e., happy, sad, neutral, or fear) influencing the intrinsic connections in an exhaustive manner (i.e. happy only; sad only; …; happy and sad only; …; etc.). The exhaustive combination of the four affects involved allowed the construction of 14 additional models. These 14 post hoc models were compared by random effects Bayesian model selection along with the original optimal model (i.e. Model 26). Parameters from the optimal model were extracted to compute endogenous connectivity and modulatory parameters (strengths), which we then statistically evaluated versus zero. These extracted parameters underwent a Pearson correlation with items mentioned earlier (i.e., intelligence, anxiety and depression, and state and trait affect), as well as results collected from the image-rating task.

Table 2
ROIs used for effective connectivity analysis.

	MNI Coordinates			
Anatomical Label (ROI Label)	x	y	z	Cluster Size
A				
R Inferior Occipital Gyrus	50	−72	−2	1300
L Inferior Occipital Gyrus	−48	−72	4	680
L Fusiform	−42	−52	−18	68
R Inferior Frontal Gyrus	42	6	26	30
B				
Pons	2.5	−25	−35	–
R Amygdala	22	−3	−17	–
L Amygdala	−20	−6	−17	–
R Orbitofrontal Cortex	36	25	−3	–
L Orbitofrontal Cortex	−38	25	−8	–
Medial Prefrontal Cortex	−4	52	31	–

(A) MNI coordinates of local maxima and corresponding cluster sizes (in voxels) for brain regions with significant activation between viewing affective and scrambled stimuli ($p_{(FWE)} = 0.05$, cluster threshold = 10 voxels) identified from the GLM. (B) MNI coordinates of the additional a-priori identified ROIs included in the effective connectivity analysis. These ROIs were generated by cross checking the a-priori literature with the significant activations between viewing affective and scrambled stimuli ($p_{(FDR)} = 0.05$).

3. Results

3.1. Tract diffusivity correlates with affective image ratings of fear

Fig. 1A displays the RGB vector map of the DTI data overlaid on the T1 image of a representative subject. Deterministic tractography was able to successfully generate fiber bundles between the optic chiasm and brain stem (Fig. 1B) and between the optic chiasm and thalamus. Although all participants were able to generate fibers, two participants had too few fibers within the bundles for successful extraction of deterministic FA. The deterministic FA values are $M = 0.29$ ($SD = 0.04$) between the optic chiasm and brain stem ($N = 60$) and M = 0.29 (SD = 0.03) between the optic chiasm and thalamus. Similarly, the probabilistic tractography algorithm successfully generated tract bundles between both sets of ROIs. The extracted FA value for fiber bundles identified between the optic chiasm and brain stem was $M = 0.33$ ($SD = 0.04$) and that for fiber bundles between the optic chiasm and thalamus was $M = 0.33$ ($SD = 0.05$). Notably, between the optic chiasm and brain stem, an additional bundle of fibers toward the pontine region was identified through probabilistic tractography but not deterministic tractography (Fig. 1C; red arrow).

From its anatomical position, this tract is likely the abducens nerve judging from the position of exit based on the four cranial nerves (V-VIII) originating from the pons. We therefore referred this tract as abducens when discussing the findings of this study.

Further analyses comparing the FA values with behavioral outcomes revealed that the deterministic FA of the fiber bundles between the optic chiasm and brain stem was significantly correlated with arousal ratings of fear stimuli [$r(60) = 0.41$, $p_{(FWE)} < 0.05$] and fear ratings of fear stimuli only [$r(60) = 0.39$, $p_{(FWE)} < 0.05$]. Individual subject data are shown in the scatterplots in Fig. 2. In Table 3, we summarize the correlation values between deterministic FA (optic chiasm and the brain stem) and all measured variables, along with their statistical probabilities. The Bonferroni correction was applied to correct for the comparison with all 17 measured variables as described in the Supplementary Materials and summarized in Table 1. The deterministic and probabilistic FA of these same fiber bundles were unable to predict age, anxiety, depression, intelligence, and state and trait affective measures. Both deterministic and probabilistic FA of the fiber bundles between the optic chiasm and thalamus were unable to predict any behavioral and demographic measures.

3.2. The pons is involved in the earliest stage of visual affective processing

Results from the whole-brain GLM contrast comparing the responses for intact affective images versus scrambled images at initial thresholding ($p_{(FDR)} = 0.05$) revealed activity in a number of regions consistent with those identified in previous work (Hadjikhani and de Gelder, 2003; Hamann, 2011; Jastorff et al., 2015; Kragel and LaBar, 2016; Lindquist et al., 2015). Applying a further stringent threshold ($p_{(FWE)} = 0.05$, cluster threshold = 10 voxels) resulted in four main clusters across both hemispheres that responded significantly differently between the two sets of stimuli (Table 2A). These clusters were identified as the bilateral inferior occipital gyrus (IOG; Fig. 3A), the left fusiform gyrus (Fig. 3B), and the right inferior frontal gyrus (IFG; Fig. 3C). Two of the identified clusters formed the bilateral IOG, which were then grouped into a single ROI for parameter extraction in the effective connectivity analyses. Although the beta values extracted from these ROIs were significantly correlated with various behavioral affective measures (i.e. arousal or valence ratings) at a $p < 0.05$ level, none of them survived Bonferroni correction.

We included a total of seven regions (Table 2) in subsequent DCM (SPM12) analyses. Bayesian model selection indicated that the most optimal of the initial 75 models (Model 26, Fig. 4) had a family expected probability of 0.150 and family exceedance probability of 0.997. Other models had family expected probabilities below 0.04 and family exceedance probabilities below 0.003. We generated 14 additional models based on identical intrinsic connections in Model 26 by exhaustively varying the combinations of affective modulation (i.e., happy, sad, neutral, or fear) to determine whether this network has affect specificity. Bayesian model selection indicated that Model 26 remained the optimal model, with a family expected probability of 0.614 and family exceedance probability of 1, whereas all other models had family expected probabilities below 0.1 and family exceedance probabilities of zero.

Model 26 has an intrinsic structure that contains unidirectional connections outward from the pons toward all other ROIs (Fig. 4). Among these unidirectional connections, the extracted parameters indicated that only the intrinsic connections from the pons to the left fusiform and the intrinsic connections from the pons to the right IFG were significantly different from zero (Fig. 4). The parameters extracted for the intrinsic self-connections for the amygdala, IOG, OFC, left fusiform, and right IFG were all significantly different from zero.

Modulation of affect was observed only on the intrinsic pathways exiting the pons (including the intrinsic self-connection), rather than all intrinsic connections specified in Model 26. Direct modulations of affect to the ROIs were only present for the a-priori and literature-identified ROIs. We summarized all modulatory parameters in Fig. 5 for each of the four types of affective stimuli. The parameters for the direct modulation of the OFC and mPFC were significantly different from zero for all affective stimuli. The strength of the direct modulation of the pons and amygdala was only significantly different from zero for neutral and sad stimuli. The modulatory strength of the intrinsic self-connection pathway of the pons was positively significantly different from zero for all four affect types. Happy affective stimuli displayed no significant modulation on any of the intrinsic pathways between pons and the other ROIs. The modulatory strength of the pons-to-left-fusiform connection by fear and sad stimuli was significantly different from zero. The modulatory parameters on the pons-to-mPFC connection by neutral and sad stimuli, as well as on the pons-to-amygdala by neutral stimulus, were significantly different from zero. We did not observe a significant modulation by affect type for the pons-to-IOG, pons-to-right-IFG, and pons-to-OFC connections.

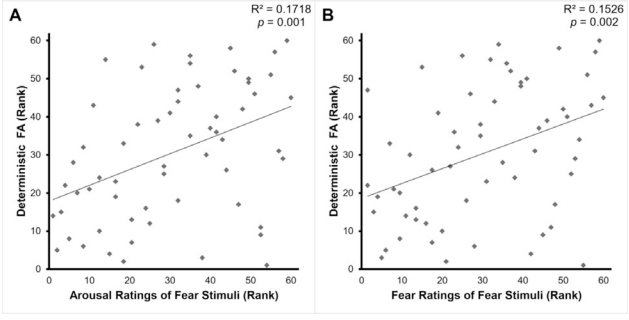

Fig. 2. Scatterplots of deterministic FA between the optic chiasm and the brain stem against arousal and fear ratings of fear stimuli.
(**A**) Scatterplot of deterministic FA between the optic chiasm and the brain stem (excluding superior colliculi) against the arousal ratings of fear stimuli. (**B**) Scatterplot of deterministic FA between the optic chiasm and the brain stem (excluding superior colliculi) against the fear ratings of fear stimuli.

Table 3
Spearman's rho correlation coefficient between all measured variables and the deterministic FA between the optic chiasm and the brain stem.

Variables	Spearman's rho	*p*
Age (year)	−0.03	0.80
General intelligence (TONI-4)	−0.13	0.34
HADS-Anxiety	0.03	0.83
HADS-Depression	−0.08	0.54
CAS-Positive affect	−0.20	0.13
CAS-Negative affect	0.03	0.83
Arousal ratings		
Happy stimuli	0.25	0.06
Sad stimuli	0.34	0.01
Fear stimuli	0.41	0.00*
Neutral stimuli	0.22	0.09
Valence ratings		
Happy stimuli	0.27	0.04
Sad stimuli	−0.05	0.69
Fear stimuli	−0.12	0.36
Neutral stimuli	0.16	0.23
Happy ratings for happy stimuli	0.09	0.48
Sad ratings for sad stimuli	0.28	0.03
Fear ratings for fear stimuli	0.39	0.00*

The Spearman's rho correlation coefficient and the corresponding probability calculated between all measured variables and the deterministic FA between the optic chiasm and the brain stem (excluding superior colliculi) for 60 participants. $^{*}p_{(FWE)} < 0.05$.

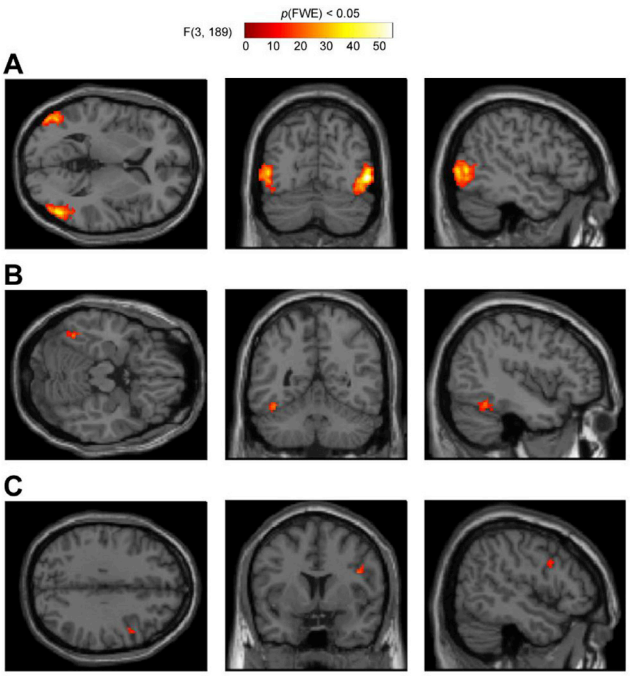

Fig. 3. Comparison results from the whole-brain GLM for responses to the intact affective images versus the scrambled images.
Significant clusters are indicated by colors on the scale bar ($p_{(FWE)} = 0.05$, cluster threshold = 10 voxels) reflecting the corresponding F-values. (**A**) Significant activations in the bilateral inferior occipital gyrus (IOG) between viewing affective and scrambled stimuli. (**B**) Significant activations in the left fusiform between viewing affective and scrambled stimuli. (**C**) Significant activations in the right inferior frontal gyrus (IFG) between viewing affective and scrambled stimuli.

4. Discussion

Using deterministic and probabilistic tractography, we identified fiber tracts between the optic chiasm and the brain stem (towards the

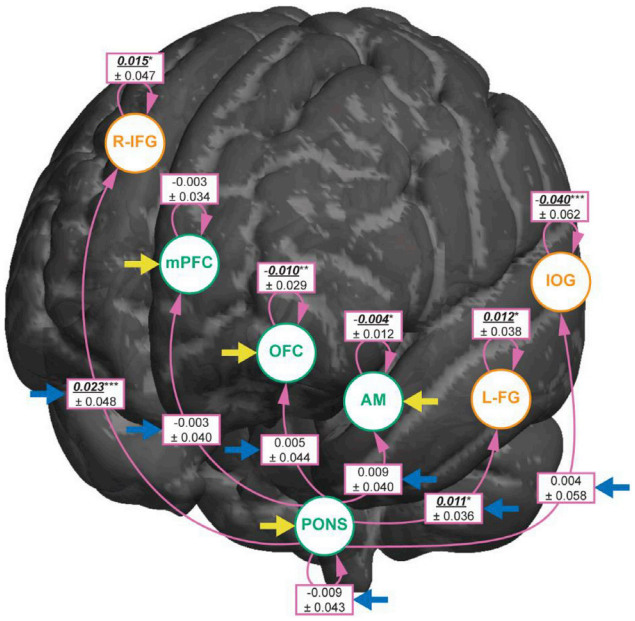

Fig. 4. The optimal model (Model 26) from Bayesian model selection.
GLM-identified ROIs are indicated by orange circles and text (Table 2**A**), whereas a-priori and literature-based ROIs are indicated by green circles and text (Table 2**B**). Pink arrows indicate the direction of the intrinsic connections, blue arrows indicate the intrinsic connections modulated by affect, and yellow arrows indicate the direct modulation on the ROIs by affect. Numbers within the pink boxes in black font are the extracted intrinsic endogenous connectivity parameters and standard deviations. Bold and underlined values indicate the respective significance: $^{*}p < 0.05$, $^{**}p < 0.01$, $^{***}p < 0.001$. AM = bilateral amygdala; IOG = bilateral inferior occipital gyrus; L-FG = left fusiform; mPFC = medial prefrontal cortex; OFC = bilateral orbitofrontal cortex; R-IFG = right inferior frontal gyrus.

posterior part of the pons). From the four cranial nerves (V-VIII) which originate from the pons, we inferred that the (probabilistic) tractography output is the abducens nerve judging from its position of exit, shape, and known connection with extraocular muscles. Both methods of tractography identified the optic tract between the optic chiasm and the thalamus, reaffirming the reliability of the DWI data as well as the tractography parameters.

We found that tract FA between the optic chiasm and brain stem only correlated to behavioral affective judgement of arousal and fear pertaining to fear affective stimuli. The lack of correlation between the FA of the abducens with judgements of other affective stimuli and baseline measures (i.e. state and trait affect, anxiety, depression, and intelligence indexes), suggest that this tract may contribute to the processing of (fearful) visual-affective stimuli. This finding is particularly interesting in light of the fact that FA retrieved from the classical retinogeniculo tract (i.e., the optic tract) did not correlate with affect judgments nor baseline measures, suggesting that the chiasm to brain stem tract may carry functions pertaining to affective processing. To our knowledge, the only study to date that has explored the relationship between diffusion measures and affective recognition showed that fiber density between the pulvinar and amygdala was correlated with the ability to recognize faces of fear (McFadyen et al., 2019). Our findings suggest that the abducens may have a role in the delivery of fear related visual affective information to the pons, which coincided with that of the rodents.

The tractography findings, specifically the relevance of a brain stem-originating tract (abducens) for affective processing, are exciting because they add a missing puzzle piece to the knowledge of a cortico-limbic network for affective processing—that is, visual-affective processing

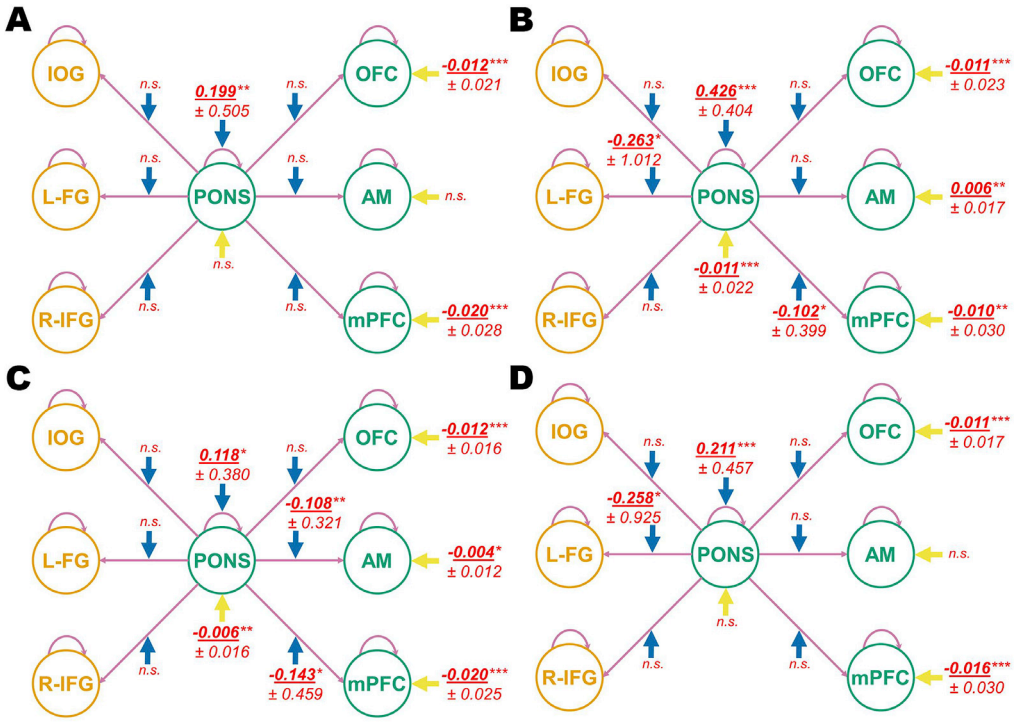

Fig. 5. Modulatory parameters on the optimal model (Model 26) from Bayesian model selection.
Blue arrows indicate the modulation on intrinsic connections, and yellow arrows indicate the direct modulation on the ROI. Numbers beside each arrow indicate the corresponding modulatory parameters and standard deviations extracted for (**A**) happy affective stimuli, (**B**) sad affective stimuli, (**C**) neutral affective stimuli, and (**D**) fearful affective stimuli. The bold font indicates values that are significant when compared to zero while n.s. indicates non-significant values. Asterisks indicate the following levels of significance: $*p < 0.05$, $**p < 0.01$, $***p < 0.001$. AM = bilateral amygdala; IOG = bilateral inferior occipital gyrus; L-FG = left fusiform; mPFC = medial prefrontal cortex; OFC = bilateral orbitofrontal cortex; R-IFG = right inferior frontal gyrus.

involves a phylogenetically older locus in the pons. Previous findings have shown that early eye gaze is more sensitive to affective than affectively neutral stimuli (Calvo and Lang, 2004). In visual search tasks, affectively negative stimuli have been shown to be detected faster among distractors than neutral or positive stimuli (Fox et al., 2000). Our results showing that the abducens, a somatic efferent responsible for driving gaze behavior, to be particularly sensitive to fear affective stimuli resonate with our instinctive needs for natural survival. The fact that our eye movements are sensitive to fear affective stimuli offers rapid evaluation of ecologically relevant stimuli, leading to their preferential access to awareness that benefits survival by allowing prompt responses to potential dangers.

Results from the DCM analyses showing task-dependent interactions between brain regions clearly pointed toward an optimal model (Model 26, Fig. 4) that comprised only of outward connections from the pontine region towards other ROIs (i.e., amygdala, IOG, OFC, mPFC, left fusiform, and right IFG). The implication of the pons for affective processing is consistent with previous work showing the involvement of this region during the passive viewing of affective stimuli, wherein the affect states also modulated the functional connectivity between the pons and other brain regions (Lee et al., 2015). The present data take these findings a step further, however, by placing the functional role of the pons in the earliest stage of visual-affective processing. We observed that the left fusiform and right IFG were both targets of significant intrinsic connections from the pons, as well as having significant self-connections, respectively, which is consistent with previous findings (Sabatinelli et al., 2011). The fusiform has been implicated in the processing of emotional facial expressions (Harry et al., 2013; Ho et al., 2016), whereas activity of the IFG correlates with the perception of emotions (Hafeman et al., 2014; Tabei ,2015). In the case of the current study, fusiform activity may also be partly driven by an over-representation of faces in the happy and sad stimuli as opposed to the neutral and fear stimuli. Although the amygdala, IOG, and OFC did not receive significant projections from the pons, they all possess significant intrinsic self-connections, indicating their relevance for affective processing, although not as direct targets from the pons. The above findings add valuable insight to the already scarce research on the functional role of the pontine regions in affective processing. The direct projection from the optic chiasm to brain stem regions, specifically to the pons, may underpin the very fast and prompt response via directing eye gaze to the perceived dangerous stimuli before our conscious awareness and evaluation of the stimuli. If better understood, the tract may be the key to understanding hypervigilance that underpins clinical pathology such as panic attacks and posttraumatic stress disorders. Our findings further emphasize the role of deeper, subcortical structures of the brain for affective processing by critically showing that the pons seem to be particularly relevant for the processing of negative (i.e., sad and fear), but not positive affective stimuli.

We note that the optimal model (Model 26, Fig. 4) displayed no affect specificity and that all four affects (i.e., happy, sad, neutral, or fear) are relevant. The extracted modulatory strengths (Fig. 5) on the pontine intrinsic self-connection pathways by all affects were positively significantly different from zero, emphasizing its relevance in processing visual affective information. However, when looking specifically at the extracted modulation parameters on the intrinsic connections projecting from the pons, there is evidence of affect specificity given that fear, neutral, and sad stimuli each possessed at least one modulatory strength that was significantly different from zero, whereas the happy stimuli did not (Fig. 5). The targets of the significant modulated projections are the amygdala, fusiform, and mPFC, which are all well documented in

processing affective stimuli (Britton et al., 2008; Geday et al., 2003; Gerber et al., 2008). We speculate that the negative specificity identified in humans is arguably consistent with the findings from the gerbils (Huang et al., 2017) because only affectively neutral and sad stimuli were reliably tested in Huang's study. Considering the DTI findings that the abducens is responsible for delivering only fear related information to the pons, these DCM findings also imply that an alternative pathway is responsible for the delivery of sad information. Future studies should aim to elucidate the differences in networks involved with the pons when processing fear versus sad stimuli.

There are some cautionary notes. To acquire 30 diffusion direction DTI images in high resolution while maintaining a reasonable total experiment duration, we scanned the partial brain focusing on the optic chiasm and the pontine region as opposed to the whole brain. This limitation on the field of view (FOV) might have influenced the number of tracts identified through tractography. In order to maintain consistency for our fMRI task, all of our affective stimuli need to be still images rather than animations or videos. Future studies should explore whether differences in the delivery of stimuli, such as using looming stimuli in the case of fear, would lead to any differences. Although the valence ratings were significantly different between the affect categories we note that the distribution of ratings were rather narrow. We postulate this to be related to the fact that our participants were all healthy Chinese adults, which has been reported to display less emotional expressions and exhibit less emotional intensity when viewing facial expressions posed by other races (Ekman et al., 1987; Matsumoto, 1993; Soto et al., 2005). Future studies should aim to extend the study to a broader group of participants, as well as adapt the choice of stimuli to correspond to the ethnicity of the participants. Related to the selection of stimuli, future studies should also aim to achieve better balance over the different visual elements (i.e. faces, animals, etc.) within each category of affective stimuli to reduce the differences caused by irrelevant components. We only studied a single group of healthy and young adults, thus limiting the range of analyses and understanding of age-related changes of this network. Furthermore, as affective processing has also been implicated in major depressive disorders, studying a clinical sample may shed light on the maintenance of affective stability.

5. Conclusions

In this research, we make an important contribution to affective neuroscience, as we exemplify a rarely studied yet pivotal brain region implicated in the early stages of visual-affective processing. Our tractography findings suggest that well-established tracts between the optic chiasm and the brain stem may function outside their conventional domain to play a role in affective processing. The functional architecture of the affective processing network revealed here clearly pointed at the important role played by brain stem regions in visual-affective processing. Future studies employing ecologically valid and intense fear stimuli would help verify the relationship between fear and intrinsic connections between the pons and all other ROIs, and they would offer significant insight into the neural basis of normal and pathological responses to fear stimuli.

Declaration of competing interest

The funder of the study had no role in study design, data collection, data analysis, data interpretation, or the writing of the report. All authors had access to the data, and all authors agreed to submit the paper for publication.

CRediT authorship contribution statement

Jing Jun Wong: Writing - original draft, Writing - review & editing, Data curation, Formal analysis. **Dorita H.F. Chang:** Formal analysis, Writing - original draft, Writing - review & editing. **Di Qi:** Data curation. **Weiwei Men:** Data curation. **Jia-Hong Gao:** Conceptualization, Data curation. **Tatia M.C. Lee:** Conceptualization, Funding acquisition, Writing - original draft, Writing - review & editing, Supervision.

Acknowledgements

The project was supported by The University of Hong Kong May Endowed Professorship in Neuropsychology and the Science and Technology Program of Guangdong (2018B030334001). The authors also thank the National Center for Protein Sciences at Peking University in Beijing, China, for assistance with MRI data acquisition and data analyses.

Appendix A. Supplementary data

Supplementary data to this article can be found online at https://doi.org/10.1016/j.neuroimage.2020.116692.

References

Aarsland, D., Marsh, L., Schrag, A., 2009. Neuropsychiatric symptoms in Parkinson's disease. Mov. Disord. 24, 2175–2186. https://doi.org/10.1002/mds.22589.
Adolphs, R., 2008. Fear, faces, and the human amygdala. Curr. Opin. Neurobiol. 18, 166–172.
Adolphs, R., 2002. Neural systems for recognizing emotion. Curr. Opin. Neurobiol. 12, 169–177. https://doi.org/10.1016/S0959-4388(02)00301-X.
Arif, H., Mohr, J.P., Elkind, M.S., 2005. Stimulus-induced pathologic laughter due to basilar artery dissection. Neurology 64, 2154–2155.
Atsak, P., Orre, M., Bakker, P., Cerliani, L., Roozendaal, B., Gazzola, V., Moita, M., Keysers, C., 2011. Experience modulates vicarious freezing in rats: a model for empathy. PloS One 6, e21855. https://doi.org/10.1371/journal.pone.0021855.
Baroncini, M., Jissendi, P., Balland, E., Besson, P., Pruvo, J.-P., Francke, J.-P., Dewailly, D., Blond, S., Prevot, V., 2012. MRI atlas of the human hypothalamus. Neuroimage 59, 168–180.
Basser, P.J., Pajevic, S., Pierpaoli, C., Duda, J., Aldroubi, A., 2000. In vivo fiber tractography using DT-MRI data. Magn. Reson. Med. 44, 625–632.
Berger, M., Gray, J.A., Roth, B.L., 2009. The expanded biology of serotonin. Annu. Rev. Med. 60, 355–366. https://doi.org/10.1146/annurev.med.60.042307.110802.
Bradley, M.M., Lang, P.J., 1994. Measuring emotion: the self-assessment manikin and the semantic differential. J. Behav. Ther. Exp. Psychiatr. 25, 49–59.
Brainard, D.H., 1997. The psychophysics toolbox. Spatial Vis. 10, 433–436.
Britton, J.C., Shin, L.M., Barrett, L.F., Rauch, S.L., Wright, C.I., 2008. Amygdala and fusiform gyrus temporal dynamics: responses to negative facial expressions. BMC Neurosci. 9, 44.
Calvo, M.G., Lang, P.J., 2004. Gaze patterns when looking at emotional pictures: motivationally biased attention. Motiv. Emot. 28, 221–243.
Canli, T., Lesch, K.-P., 2007. Long story short: the serotonin transporter in emotion regulation and social cognition. Nat. Neurosci. 10, 1103–1109. https://doi.org/10.1038/nn1964.
Cardinal, R.N., Parkinson, J.A., Hall, J., Everitt, B.J., 2002. Emotion and motivation: the role of the amygdala, ventral striatum, and prefrontal cortex. Neurosci. Biobehav. Rev. 26, 321–352. https://doi.org/10.1016/S0149-7634(02)00007-6.
Davis, M., Whalen, P.J., 2001. The amygdala: vigilance and emotion. Mol. Psychiatr. 6, 13–34. https://doi.org/10.1038/sj.mp.4000812.
Desikan, R.S., Ségonne, F., Fischl, B., Quinn, B.T., Dickerson, B.C., Blacker, D., Buckner, R.L., Dale, A.M., Maguire, R.P., Hyman, B.T., others, 2006. An automated labeling system for subdividing the human cerebral cortex on MRI scans into gyral based regions of interest. Neuroimage 31, 968–980.
Deutsch, G.K., Dougherty, R.F., Bammer, R., Siok, W.T., Gabrieli, J.D.E., Wandell, B., 2005. Children's reading performance is correlated with white matter structure measured by diffusion tensor imaging. Cortex 41, 354–363. https://doi.org/10.1016/S0010-9452(08)70272-7.
Ekman, P., Friesen, W.V., O'sullivan, M., Chan, A., Diacoyanni-Tarlatzis, I., Heider, K., Krause, R., LeCompte, W.A., Pitcairn, T., Ricci-Bitti, P.E., 1987. Universals and cultural differences in the judgments of facial expressions of emotion. J. Pers. Soc. Psychol. 53, 712.
Ellenbroek, B., Youn, J., 2016. Rodent models in neuroscience research: is it a rat race? Dis. Model. Mech. 9, 1079–1087. https://doi.org/10.1242/dmm.026120.
Fox, E., Lester, V., Russo, R., Bowles, R., Pichler, A., Dutton, K., 2000. Facial expressions of emotion: are angry faces detected more efficiently? Cognit. Emot. 14, 61–92.
Frazier, J.A., Chiu, S., Breeze, J.L., Makris, N., Lange, N., Kennedy, D.N., Herbert, M.R., Bent, E.K., Koneru, V.K., Dieterich, M.E., others, 2005. Structural brain magnetic resonance imaging of limbic and thalamic volumes in pediatric bipolar disorder. Am. J. Psychiatr. 162, 1256–1265.
Friston, K., Mattout, J., Trujillo-Barreto, N., Ashburner, J., Penny, W., 2007. Variational free energy and the Laplace approximation. Neuroimage 34, 220–234.
Friston, K.J., Harrison, L., Penny, W., 2003. Dynamic causal modelling. Neuroimage 19, 1273–1302.

Geday, J., Gjedde, A., Boldsen, A.-S., Kupers, R., 2003. Emotional valence modulates activity in the posterior fusiform gyrus and inferior medial prefrontal cortex in social perception. Neuroimage 18, 675–684.
Gerber, A.J., Posner, J., Gorman, D., Colibazzi, T., Yu, S., Wang, Z., Kangarlu, A., Zhu, H., Russell, J., Peterson, B.S., 2008. An affective circumplex model of neural systems subserving valence, arousal, and cognitive overlay during the appraisal of emotional faces. Neuropsychologia 46, 2129–2139.
Goldstein, J.M., Seidman, L.J., Makris, N., Ahern, T., O'Brien, L.M., Caviness Jr., V.S., Kennedy, D.N., Faraone, S.V., Tsuang, M.T., 2007. Hypothalamic abnormalities in schizophrenia: sex effects and genetic vulnerability. Biol. Psychiatr. 61, 935–945.
Hadjikhani, N., de Gelder, B., 2003. Seeing fearful body expressions activates the fusiform cortex and amygdala. Curr. Biol. 13, 2201–2205. https://doi.org/10.1016/j.cub.2003.11.049.
Hafeman, D.M., Bebko, G., Bertocci, M.A., Fournier, J.C., Bonar, L., Perlman, S.B., Travis, M., Gill, M.K., Diwadkar, V.A., Sunshine, J.L., others, 2014. Abnormal deactivation of the inferior frontal gyrus during implicit emotion processing in youth with bipolar disorder: attenuated by medication. J. Psychiatr. Res. 58, 129–136.
Halliday, G.M., Li, Y.W., Blumbergs, P.C., Joh, T.H., Cotton, R.G.H., Howe, P.R.C., Blessing, W.W., Geffen, L.B., 1990. Neuropathology of immunohistochemically identified brainstem neurons in Parkinson's disease. Ann. Neurol. 27, 373–385. https://doi.org/10.1002/ana.410270405.
Hamann, S., 2011. Affective neuroscience: amygdala's role in experiencing fear. Curr. Biol. 21, R75–R77. https://doi.org/10.1016/j.cub.2010.12.007.
Harry, B.B., Williams, M., Davis, C., Kim, J., 2013. Emotional expressions evoke a differential response in the fusiform face area. Front. Hum. Neurosci. 7, 692.
Ho, T.C., Zhang, S., Sacchet, M.D., Weng, H., Connolly, C.G., Henje Blom, E., Han, L.K., Mobayed, N.O., Yang, T.T., 2016. Fusiform gyrus dysfunction is associated with perceptual processing efficiency to emotional faces in adolescent depression: a model-based approach. Front. Psychol. 7, 40.
Hoptman, M.J., Ardekani, B.A., Butler, P.D., Nierenberg, J., Javitt, D.C., Lim, K.O., 2004. DTI and impulsivity in schizophrenia: a first voxelwise correlational analysis. Neuroreport 15, 2467–2470. https://doi.org/10.1097/00001756-200411150-00007.
Hu, B., Ye, B., Yang, Y., Zhu, K., Kang, Z., Kuang, S., Luo, L., Shan, H., 2011. Quantitative diffusion tensor deterministic and probabilistic fiber tractography in relapsing–remitting multiple sclerosis. Eur. J. Radiol. 79, 101–107. https://doi.org/10.1016/j.ejrad.2009.11.021.
Huang, L., Yuan, T., Tan, M., Xi, Y., Hu, Y., Tao, Q., Zhao, Z., Zheng, J., Han, Y., Xu, F., others, 2017. A retinoraphe projection regulates serotonergic activity and looming-evoked defensive behaviour. Nat. Commun. 8, 14908.
Jastorff, J., Huang, Y.-A., Giese, M.A., Vandenbulcke, M., 2015. Common neural correlates of emotion perception in humans. Hum. Brain Mapp. 36, 4184–4201.
Jeon, D., Kim, S., Chetana, M., Jo, D., Ruley, H.E., Lin, S.-Y., Rabah, D., Kinet, J.-P., Shin, H.-S., 2010. Observational fear learning involves affective pain system and Cav1.2 Ca2+ channels in ACC. Nat. Neurosci. 13, 482–488. https://doi.org/10.1038/nn.2504.
Jubault, T., Brambati, S.M., Degroot, C., Kullmann, B., Strafella, A.P., Lafontaine, A.-L., Chouinard, S., Monchi, O., 2009. Regional brain stem atrophy in idiopathic Parkinson's disease detected by anatomical MRI. PloS One 4. https://doi.org/10.1371/journal.pone.0008247 e8247–e8247.
Kragel, P.A., LaBar, K.S., 2016. Decoding the nature of emotion in the brain. Trends Cognit. Sci. 20, 444–455.
Lau, B.W.-M., Ren, C., Yang, J., Yan, S.W., Chang, R.C.-C., Pu, M., So, K.-F., 2011. Light deprivation induces depression-like behavior and suppresses neurogenesis in diurnal Mongolian gerbil (Meriones unguiculatus). Cell Transplant. 20, 871–882.
Lee, T.M., Cheung, C.C., Lau, E.Y., Mak, A., Li, L.S., 2003. Cognitive and emotional dysfunction after central pontine myelinolysis. Behav. Neurol. 14, 103–107.
Lee, T.M., Sun, D., Wong, N.M., Shao, R., Men, W., Ge, J., So, K.-F., Gao, J.-H., Chan, C.C., 2015. A pontine region is a neural correlate of the human affective processing network. EBioMedicine 2, 1799–1805.
Li, X., Ren, C., Huang, L., Lin, B., Pu, M., Pickard, G.E., So, K.-F., 2015. The dorsal raphe nucleus receives afferents from alpha-like retinal ganglion cells and intrinsically photosensitive retinal ganglion cells in the rat. Invest. Ophthalmol. Vis. Sci. 56, 8373–8381.
Lindquist, K.A., Satpute, A.B., Wager, T.D., Weber, J., Barrett, L.F., 2015. The brain basis of positive and negative affect: evidence from a meta-analysis of the human neuroimaging literature. Cerebr. Cortex 26, 1910–1922.
Luan, L., Ren, C., Lau, B.W.-M., Yang, J., Pickard, G.E., So, K.-F., Pu, M., 2011. Y-like retinal ganglion cells innervate the dorsal raphe nucleus in the Mongolian gerbil (Meriones unguiculatus). PloS One 6, e18938.
Makris, N., Goldstein, J.M., Kennedy, D., Hodge, S.M., Caviness, V.S., Faraone, S.V., Tsuang, M.T., Seidman, L.J., 2006. Decreased volume of left and total anterior insular lobule in schizophrenia. Schizophr. Res. 83, 155–171.
Marchewka, A., Żurawski, Ł., Jednoróg, K., Grabowska, A., 2014. The Nencki Affective Picture System (NAPS): introduction to a novel, standardized, wide-range, high-quality, realistic picture database. Behav. Res. Methods 46, 596–610.
Matsumoto, D., 1993. Ethnic differences in affect intensity, emotion judgments, display rule attitudes, and self-reported emotional expression in an American sample. Motiv. Emot. 17, 107–123. https://doi.org/10.1007/BF00995188.
Mazziotta, J., Toga, A., Evans, A., Fox, P., Lancaster, J., Zilles, K., Woods, R., Paus, T., Simpson, G., Pike, B., Holmes, C., Collins, L., Thompson, P., MacDonald, D., Iacoboni, M., Schormann, T., Amunts, K., Palomero-Gallagher, N., Geyer, S., Parsons, L., Narr, K., Kabani, N., Goualher, G.L., Boomsma, D., Cannon, T., Kawashima, R., Mazoyer, B., 2001. A probabilistic atlas and reference system for the human brain: international Consortium for Brain Mapping (ICBM). Philos. Trans. R. Soc. Lond. B Biol. Sci. 356, 1293–1322. https://doi.org/10.1098/rstb.2001.0915.
McFadyen, J., Mattingley, J.B., Garrido, M.I., 2019. An afferent white matter pathway from the pulvinar to the amygdala facilitates fear recognition. eLife 8, e40766.
Mori, S., Crain, B.J., Chacko, V.P., Van Zijl, P.C., 1999. Three-dimensional tracking of axonal projections in the brain by magnetic resonance imaging. Ann. Neurol. Off. J. Am. Neurol. Assoc. Child Neurol. Soc. 45, 265–269.
Nobuhara, K., Okugawa, G., Sugimoto, T., Minami, T., Tamagaki, C., Takase, K., Saito, Y., Sawada, S., Kinoshita, T., 2006. Frontal white matter anisotropy and symptom severity of late-life depression: a magnetic resonance diffusion tensor imaging study. J. Neurol. Neurosurg. Amp Psychiatry 77, 120. https://doi.org/10.1136/jnnp.2004.055129.
Parvizi, J., Coburn, K.L., Shillcutt, S.D., Coffey, C.E., Lauterbach, E.C., Mendez, M.F., 2009. Neuroanatomy of pathological laughing and crying: a report of the American neuropsychiatric association committee on research. J. Neuropsychiatry Clin. Neurosci. 21, 75–87.
Pelli, D.G., 1997. The VideoToolbox software for visual psychophysics: transforming numbers into movies. Spatial Vis. 10, 437–442.
Phillips, M.L., Drevets, W.C., Rauch, S.L., Lane, R., 2003. Neurobiology of emotion perception I: the neural basis of normal emotion perception. Biol. Psychiatr. 54, 504–514. https://doi.org/10.1016/S0006-3223(03)00168-9.
Press, W.H., Flannery, B.P., Teukolsky, S., Vetterling, W., 1988. Numerical Recipes in C: the Art of Numerical Computing. Cambridge University Press.
Ren, C., Luan, L., Lau, B.W.-M., Huang, X., Yang, J., Zhou, Y., Wu, X., Gao, J., Pickard, G.E., So, K.-F., others, 2013. Direct retino-raphe projection alters serotonergic tone and affective behavior. Neuropsychopharmacology 38, 1163.
Riegel, M., Żurawski, Ł., Wierzba, M., Moslehi, A., Klocek, Ł., Horvat, M., Grabowska, A., Michałowski, J., Jednoróg, K., Marchewka, A., 2016. Characterization of the Nencki affective picture system by discrete emotional categories (NAPS BE). Behav. Res. Methods 48, 600–612.
Rohde, G.K., Barnett, A., Basser, P., Marenco, S., Pierpaoli, C., 2004. Comprehensive approach for correction of motion and distortion in diffusion-weighted MRI. Magn. Reson. Med. Off. J. Int. Soc. Magn. Reson. Med. 51, 103–114.
Rolls, E.T., 2004. The functions of the orbitofrontal cortex. Dev. Orbitofrontal Funct. 55, 11–29. https://doi.org/10.1016/S0278-2626(03)00277-X.
Sabatinelli, D., Fortune, E.E., Li, Q., Siddiqui, A., Krafft, C., Oliver, W.T., Beck, S., Jeffries, J., 2011. Emotional perception: meta-analyses of face and natural scene processing. Neuroimage 54, 2524–2533.
Saeed, U., Compagnone, J., Aviv, R.I., Strafella, A.P., Black, S.E., Lang, A.E., Masellis, M., 2017. Imaging biomarkers in Parkinson's disease and Parkinsonian syndromes: current and emerging concepts. Transl. Neurodegener. 6, 8. https://doi.org/10.1186/s40035-017-0076-6.
Sarwar, T., Ramamohanarao, K., Zalesky, A., 2019. Mapping connectomes with diffusion MRI: deterministic or probabilistic tractography? Magn. Reson. Med. 81, 1368–1384. https://doi.org/10.1002/mrm.27471.
Schlaier, J.R., Beer, A.L., Faltermeier, R., Fellner, C., Steib, K., Lange, M., Greenlee, M.W., Brawanski, A.T., Anthofer, J.M., 2017. Probabilistic vs. deterministic fiber tracking and the influence of different seed regions to delineate cerebellar-thalamic fibers in deep brain stimulation. Eur. J. Neurosci. 45, 1623–1633. https://doi.org/10.1111/ejn.13575.
Seidel, K., Mahlke, J., Siswanto, S., Krüger, R., Heinsen, H., Auburger, G., Bouzrou, M., Grinberg, L.T., Wicht, H., Korf, H.-W., den Dunnen, W., Rüb, U., 2015. The brainstem pathologies of Parkinson's disease and dementia with Lewy bodies. Brain Pathol. Zurich Switz. 25, 121–135. https://doi.org/10.1111/bpa.12168.
Sherbondy, A.J., Dougherty, R.F., Ben-Shachar, M., Napel, S., Wandell, B.A., 2008. ConTrack: finding the most likely pathways between brain regions using diffusion tractography. J. Vis. 8, 15–15.
Silveri, M.M., Rohan, M.L., Pimentel, P.J., Gruber, S.A., Rosso, I.M., Yurgelun-Todd, D.A., 2006. Sex differences in the relationship between white matter microstructure and impulsivity in adolescents. Magn. Reson. Imaging 24, 833–841. https://doi.org/10.1016/j.mri.2006.03.012.
Snyder, J.M., Hagan, C.E., Bolon, B., Keene, C.D., 2018. 20 - nervous system. In: Treuting, P.M., Dintzis, S.M., Montine, K.S. (Eds.), Comparative Anatomy and Histology, second ed. Academic Press, San Diego, pp. 403–444. https://doi.org/10.1016/B978-0-12-802900-8.00020-8.
Soto, J.A., Levenson, R.W., Ebling, R., 2005. Cultures of moderation and expression: emotional experience, behavior, and physiology in Chinese Americans and Mexican Americans. Emotion 5, 154.
Starkstein, S.E., Leentjens, A.F.G., 2008. The nosological position of apathy in clinical practice. J. Neurol. Neurosurg. Amp Psychiatry 79, 1088. https://doi.org/10.1136/jnnp.2007.136895.
Stephan, K.E., Penny, W.D., Moran, R.J., den Ouden, H.E., Daunizeau, J., Friston, K.J., 2010. Ten simple rules for dynamic causal modeling. Neuroimage 49, 3099–3109.
Tabei, K., 2015. Inferior frontal gyrus activation underlies the perception of emotions, while precuneus activation underlies the feeling of emotions during music listening. Behav. Neurol. 2015.
Terburg, D., Scheggia, D., Triana del Rio, R., Klumpers, F., Ciobanu, A.C., Morgan, B., Montoya, E.R., Bos, P.A., Giobellina, G., van den Burg, E.H., de Gelder, B., Stein, D.J., Stoop, R., van Honk, J., 2018. The basolateral amygdala is essential for rapid escape: a human and rodent study. Cell 175, 723–735. https://doi.org/10.1016/j.cell.2018.09.028 e16.
Tzourio-Mazoyer, N., Landeau, B., Papathanassiou, D., Crivello, F., Etard, O., Delcroix, N., Mazoyer, B., Joliot, M., 2002. Automated anatomical labeling of activations in SPM using a macroscopic anatomical parcellation of the MNI MRI single-subject brain. Neuroimage 15, 273–289.
Vandewalle, G., Maquet, P., Dijk, D.-J., 2009. Light as a modulator of cognitive brain function. Trends Cognit. Sci. 13, 429–438. https://doi.org/10.1016/j.tics.2009.07.004.

Vandewalle, G., Schmidt, C., Albouy, G., Sterpenich, V., Darsaud, A., Rauchs, G., Berken, P.-Y., Balteau, E., Degueldre, C., Luxen, A., Maquet, P., Dijk, D.-J., 2007. Brain responses to violet, blue, and green monochromatic light exposures in humans: prominent role of blue light and the brainstem. PloS One 2, e1247. https://doi.org/10.1371/journal.pone.0001247.

Weintraub, D., Moberg, P.J., Duda, J.E., Katz, I.R., Stern, M.B., 2003. Recognition and treatment of depression in Parkinson's disease. J. Geriatr. Psychiatr. Neurol. 16, 178–183.

Yohn, C.N., Gergues, M.M., Samuels, B.A., 2017. The role of 5-HT receptors in depression. Mol. Brain 10. https://doi.org/10.1186/s13041-017-0306-y, 28–28.

Zhang, T., Huang, L., Zhang, L., Tan, M., Pu, M., Pickard, G.E., So, K.-F., Ren, C., 2016. ON and OFF retinal ganglion cells differentially regulate serotonergic and GABAergic activity in the dorsal raphe nucleus. Sci. Rep. 6, 26060.